Effects of bacteria-embedded polylactic acid (PLA) capsules on fracture properties of strain hardening cementitious composite (SHCC)

He, Shan; Zhang, Shizhe; Luković, Mladena; Schlangen, Erik

DOI
10.1016/j.engfracmech.2022.108480

Publication date
2022

Document Version
Final published version

Published in
Engineering Fracture Mechanics

Engineering Fracture Mechanics 268 (2022) 108480

Contents lists available at ScienceDirect

Engineering Fracture Mechanics

journal homepage: www.elsevier.com/locate/engfracmech

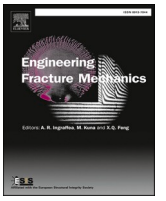

Effects of bacteria-embedded polylactic acid (PLA) capsules on fracture properties of strain hardening cementitious composite (SHCC)

Shan He [a,*], Shizhe Zhang [a], Mladena Luković [b], Erik Schlangen [a]

[a] Microlab, Faculty of Civil Engineering and Geosciences, Delft University of Technology, 2628 CN Delft, the Netherlands
[b] Concrete Structures, Faculty of Civil Engineering and Geosciences, Delft University of Technology, 2628 CN Delft, the Netherlands

ARTICLE INFO

Keywords:
Self-healing
SHCC
Fracture toughness
Elastic modulus
ITZ

ABSTRACT

Strain hardening cementitious composite (SHCC) is a special class of ultra-ductile material which has autogenous self-healing capability due to its intrinsic tight crack widths. To further improve its healing ability, healing agent (HA) can be incorporated in SHCC, enabling it also the autonomous self-healing mechanism. In this study, the effects of adding bacteria-embedded polylactic acid (PLA) capsules on the mechanical properties of SHCC with different amounts of HA (*i.e.*, 1.25%, 2.5%, 5% by weight to binder) were investigated. Experiments were conducted to examine the composite performance, matrix properties and single fiber pullout behavior of the SHCCs, followed by microscopy characterization of the fiber/matrix interface microstructure. Results show that the inclusion of the PLA-HA up to 5% by weight to binder influenced the tensile performance (*i.e.*, tensile strength and ductility) of SHCC only to a very small extent but significantly reduced the average residual crack widths. The inclusion of HA at a high dosage (5%) increased the crack tip toughness (J_{tip}) of the matrix by lowering elastic modulus and increasing fracture toughness. Single fiber pullout results show that the fiber/matrix bond properties were enhanced by the addition of the HA, which can be attributed to the formation of a denser interfacial transition zone (ITZ) with less calcium hydroxide crystals as revealed by the scanning electron microscope (SEM) micrographs. The improved bond properties led to higher fiber bridging complementary energy and thus partially sustained the tensile strain capacity as verified by the micromechanical model.

1. Introduction

Cracking in conventional reinforced concrete is usually unavoidable. It happens due to mechanical loading, early-age shrinkage, thermal effects, freeze-thaw, or a combination of these factors. Concrete having the ability to heal cracks by itself, therefore, has the prospect of exhibiting significantly improved structural and durability performance compared to other construction materials [1,2]. To promote and stimulate self-healing in concrete, extensive research has been carried out over the last decades either to stimulate the intrinsic/autogenous self-healing capacity of cementitious materials (*e.g.*, via use of mineral additives [3,4], crystalline admixtures [5,6], or superabsorbent polymers [6]), or to develop novel autonomous self-healing mechanisms (*e.g.*, via the application of micro-

* Corresponding author.
E-mail address: s.he-2@tudelft.nl (S. He).

https://doi.org/10.1016/j.engfracmech.2022.108480
Received 16 October 2021; Received in revised form 5 March 2022; Accepted 16 April 2022
Available online 21 April 2022

Nomenclature

a	notch depth of prismatic specimens for fracture toughness test
B	width of prismatic specimens for fracture toughness test
d_f	diameter of fiber
E_f	elastic modulus of fiber
E_m	elastic modulus of SHCC paste (without fiber)
F_{Max}	peak load of three-point bending test
G_d	chemical bond between fiber and SHCC matrix
J_{tip}	crack tip toughness (the critical strain energy release rate)
$J_b^{'}$	complementary energy of fiber-bridging
K_{Ic}	the stress intensity factor for mode I
K_m	matrix fracture toughness
L_e	embedded length of fiber
P_a	fiber pullout load up to full debonded length
P_b	fiber pullout load when the fiber begins to slip
$\Delta P/\Delta u$	initial slope of the pullout load vs displacement
S	loading span of fracture toughness test
V_f	fiber content in volume
W	depth of prismatic specimens for fracture toughness test
α	relative notch depth ratio
β	slip-hardening coefficient
δ	crack opening
δ_0	crack opening at fiber-bridging strength
σ	applied tensile load
σ_0	fiber-bridging strength
σ_c	matrix cracking strength
τ_0	frictional bond between fiber and SHCC matrix

[7], macro- [8], or vascular encapsulated polymers [9], minerals, or bacteria [10]). However, a critical factor that governs the healing efficiency of all self-healing pathways is the concrete crack width. It has been reported that, for autogenous healing, full crack healing can only be obtained if crack widths are less than 150 micrometers [11,12]. Even for autonomous healing, the speed and the extent to which the crack can be healed also largely depends on crack width.

Properly designed and detailed reinforcement can reduce the crack width. However, substantially high amount of steel reinforcement will be needed if the targeted crack width is up to a hundred of micrometers, which may lead to congestion of steel reinforcement and high construction complexity. Furthermore, fibers can provide an effective mean to further reduce the crack width. Among all fiber-reinforced cementitious composites (FRCCs), the Strain Hardening Cementitious Composite (SHCC) or Engineered Cementitious Composite (ECC) [13], initially developed in the 1990s based on the micro-mechanics theory [14], possesses the most desirable crack control ability as it can exhibit multiple microcracking behavior (*i.e.*, average crack width of 60–80 μm) with strain-hardening response even at a tensile strain over 3%. The unique cracking performance of SHCC is a result of careful tailoring of matrix, fiber, and matrix/fiber interface [15,16]. With given fiber, the balance between matrix and fiber/matrix interface properties plays a decisive role on the tensile and cracking performance of SHCC.

Due to the featured tight crack width, autogenous self-healing of SHCC has been the subject of extensive study. The recovery of both transport properties (*e.g.*, permeability, diffusivity, and absorptivity) and mechanical properties (*e.g.*, tensile strength, flexural strength, and strain capacity) of SHCC upon self-healing of microcracks has been experimentally confirmed under a variety of exposure environments [17]. However, it has been reported that the degree of healing in SHCC is still highly affected by the crack width. Yang et al. [4] found that the maximum allowable crack width to obtain complete resonant frequency recovery was around 50 μm; partial recovery was observed for cracks between 50 and 150 μm; cracks beyond 150 μm did not show any recovery. Fan and Li [18] studied the crack volume filling monitored by 3D X-ray computed microtomography and reported that, for cracks with width of 31 μm, the crack volume decreased by 73% after exposure to 10 wet-dry cycles. For cracks having a width of 75 μm, the reduction of crack volume under the same conditions fell to only 10.8%. In addition, it has been found that the extent of self-healing in SHCC is sensitive to the matrix composition. Qiu et al. [19] studied self-healing ability of slag based SHCC and found that the maximum allowable crack width to engage complete healing reduces with increasing the slag content. It should be noted that while SHCCs used in previous studies usually adopt high percentage of fly ash, nowadays there is a tendency to replace fly ash by slag because fly ash has large variation in chemical composition, fineness, and carbon content as well as a dwindling global availability. Irrespective of its composition, to achieve a more robust and sustainable self-healing behavior of SHCC, it would be desirable to enable SHCC the ability for healing beyond the autogenous capacity.

Incorporation of encapsulated bacterial healing agent (HA) can be one of the approaches to enable SHCC with autonomous self-healing capability. Among the various HA developed, the use of bacteria-embedded poly-lactic-acid (PLA) capsules as HA has

proven its potential to satisfy both mechanical and functional requirements of the resulting self-healing system [20,21]. The main benefit of using PLA is that it reduces the volume of required healing particles, as PLA serves not only to protect the bacterial HA as a shell but also to provide the carbon source. Previous research [21,22] has also shown promising results towards full scale application and commercialization. Nevertheless, the addition of PLA capsules can largely alter the fracture properties of the materials [23] by introducing new ITZ and by deviating crack path, possibly even increasing the crack widths and therefore having conflicting effects on self-healing ability. In addition, PLA capsules are by nature biodegradable and will partially hydrolyses in alkaline environments. It is therefore plausible that some PLA capsules may release some bacterial spore spores and nutrient medium into the fresh paste during the mixing, which may affect the mechanical properties of the cement paste. Since the tensile performance of the SHCC is the pre-requisite of adequate healing, it is important to understand the influence of HA and above-mentioned factors on the matrix and fiber/matrix bond properties of SHCC.

To address the research gaps mentioned above, this study investigates the effect of bacteria-embedded PLA capsules on the mechanical properties of SHCC. The current study does not aim to determine the optimum dosage of HA with respect to healing efficiency but focuses on understanding how the addition of the HA can affect the tensile and cracking performance of the SHCC. For this purpose, self-healing SHCC mixtures with a wide range of dosages of PLA capsules were developed; and their mechanical properties at the composite, matrix and fiber-matrix bond level were tested and compared with control SHCC without any HA. The change of matrix properties (*i.e.*, fracture toughness and elastic modulus) of the SHCCs with the use of the HA were assessed. Single fiber pullout tests were also performed to evaluate the interface bond properties between polyvinyl alcohol (PVA) fiber and the self-healing SHCC matrices. Scanning electron microscope (SEM) was used to reveal microstructural features of the interfacial transition zone (ITZ) between fiber and matrices with and without HA. Micromechanics-based models were used to calculate the fiber bridging capacity and to assess the strain-hardening potential of the resulting self-healing SHCCs.

2. Materials and tests

2.1. Mix design and materials

Table 1 shows the mixture compositions of SHCCs with varying dosages of HA (*i.e.*, 0%, 1.25%, 2.5% and 5% by weight to binder). The mix design of the control SHCC was tailored based on a SHCC mix developed in the group previously [24]. The modified SHCC matrix has a water-to-binder ratio of 0.4 and a filler-to-binder ratio of 0.5, which were determined experimentally for improved tensile strain capacity and tight crack width. Blast furnace slag (BFS) cement CEM III/B 42.5 N from ENCI (the Netherlands), consisting of 20–34 % clinker and 66–80% BFS [25], was used as binder to improve the matrix rheology and to lower matrix fracture toughness. Finely grinded limestone powder Calcitec® from Carmeuse (Belgium) with a particle size distribution similar to that of cement was used as filler to further reduce the matrix fracture toughness and to facilitate uniform fiber dispersion. A polycarboxylate-based superplasticizer MasterGlenium 51 produced from BASF (Germany) with 35.0% solid content by mass was used to reach desired workability. The fiber used in this study is PVA fiber from Kuraray (Japan) with 1.2% by weight oiling coating, the mechanical and physical properties of which are presented in Table 2.

The HA adopted in the current study is the self-healing bio-polymeric particles (Fig. 1a) produced by Basilisk (the Netherlands). It is composed of a poly-lactic acid (PLA) derivate matrix, bacterial spores of Bacillus cohnii-related strains and growth-required nutrient inorganic salts. The capsules have a particle size distribution between 0.1 to 1.0 mm (Fig. 1b).

2.2. Specimen preparation

To prepare the SHCC specimens, BFS cement and limestone powders were first dry mixed by a Hobart® mixer at low speed for 5 min. Water pre-mixed with 80% of SP was slowly added into the mixture and mixed until the fresh paste was homogenous and consistent. HAs were then gradually added and mixed for another 2 min, followed by the addition of fibers within a duration of 5 min. Meanwhile, the remaining 20% SP was added into the mixture to compensate for the rheological loss due to the addition of fibers. Afterward, the fresh SHCC was cast into polystyrene prism ($40 \times 40 \times 160$ mm^3) molds and dogbone ($80 \times 30 \times 13$ mm^3 in gauge length volume) molds, while moderate vibration was applied to remove entrapped air and to improve consolidation. The molds were then covered with plastic sheets and cured at room temperature for one day, after which the hardened specimens were removed from the molds and cured in a climate room (20 °C and ≥98% RH) for another 27 days before testing. The preparation of SHCC matrix specimens for fracture toughness test and elastic modulus test followed the same procedure except that no fiber was added into the fresh paste.

Table 1
Mixture compositions of SHCCs [unit in kg/m^3].

Mixture ID	CEM III/B	Limestone powder	Water	SP	PVA fiber (2.0 vol%)	Healing agent
SHCC-0HA	1060	530	424	2	26	0
SHCC-1.25HA	1048	524	419	2	26	13
SHCC-2.5HA	1036	518	415	2	26	26
SHCC-5HA	1014	507	406	2	26	51

Table 2
Physical and mechanical properties of PVA fibers.

Length (mm)	Diameter (μm)	Density (kg/m3)	Nominal tensile strength (MPa)	Young's modulus (GPa)	Surface oil-content (wt.%)
8	39	1300	1640	41.1	1.2

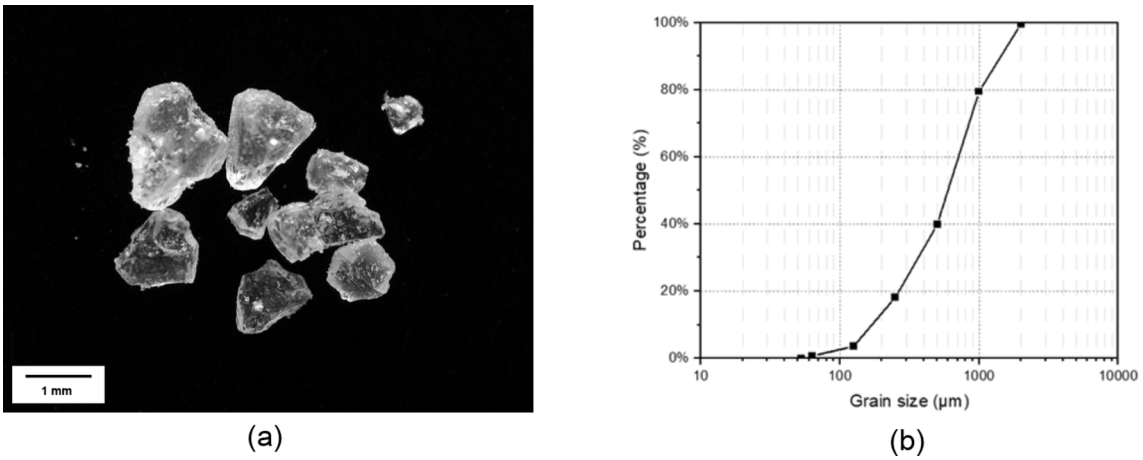

Fig. 1. (a) Photograph of bacteria-embedded PLA capsules and (b) its particle size distribution.

Preparation of single fiber pullout specimens followed the suggestion of reference [26]. A long PVA fiber was cut into about 150 mm in length and embedded into the SHCC matrices (same mix composition as in Table 1 but without the addition of PVA fiber). The hardened specimen was demolded after one day and cured in the same condition as described for the SHCC specimens. The specimens were sawed into thin specimens having 1 mm in thickness with a single fiber extruding out from one side.

2.3. Tests

The compressive strength of the SHCC was measured in accordance with NEN EN 196-1 [27] by using 40 × 40 × 40 mm^3 cube specimens. Uniaxial tension tests were performed by using a servo-hydraulic testing machine (Instron® 8872) under displacement control at a rate of 0.005 mm/s. Dogbone-shaped specimens recommended by the Japan Society of Civil Engineers (JSCE) [28] with a cross-section of 13 × 30 mm at the test zone were adopted. During tests, the specimens were glued at both ends with thick steel plates bolted to the testing machine to avoid stress concentration. The deformations were measured with a gauge length of 80 mm with two Linear Variable Differential Transformers (LVDTs) fixed on both sides of the specimens. Tests were stopped by releasing the applied tensile load after the tensile load drops to 80% of the maximum load. Immediately after the tensile test, the residual crack width of unloaded specimens was measured by using a pre-calibrated digital microscope. The maximum tensile stress experienced by the specimen during this experiment is called the ultimate tensile strength (σ_{ult}), and the corresponding strain value is called the tensile strain capacity (ε_{ult}). At least 4 samples were tested for each mixture. The average and the standard deviation of the results were reported.

The matrix properties (*i.e.*, elastic modulus and fracture toughness) of the SHCC mixtures without fiber were tested by using 40 × 40 × 160 mm^3 prismatic specimens. For each matrix property, at least 6 samples from each mixture were tested, the results of which were then summarized by calculating the average and the standard deviation. Elastic modulus test was carried out in accordance with NEN-EN 12390-13 [29] with prism specimens as shown by Fig. 3. Four LVDTs were arranged at each side of the prism along central axis of the specimen with a gauge length of 10 cm. The tests were carried out under load control at a rate of 0.1 N/s for measuring the

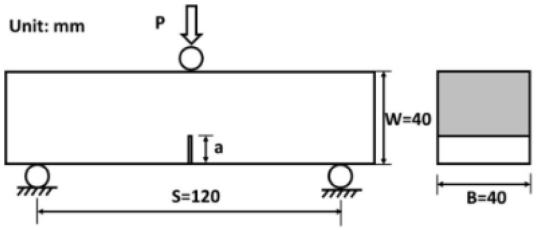

Fig. 2. Experimental set-up for fracture toughness test.

stabilized secant modulus of elasticity. Three loading cycles were carried out after preloading. The fracture toughness of SHCC matrices was determined by performing three-point bending tests on pre-notched prism specimens in accordance with the Extended Round Robin Testing program (RRT+) of COST ACTION TU1404 [30]. The notches with a thickness of 1.5 mm and a depth of 12 mm were prepared by using a cutting saw. Bending tests were performed under crack mouth opening displacement (CMOD) control at a rate of 0.01 mm/min, which was monitored by two LVDTs on both sides of the notch. The prism was supported over a load span of 120 mm. The detailed testing set-up is shown in Fig. 2. Since SHCC matrix formulations do not contain coarse aggregates, the fracture process zone size is expected to be small compared with all relevant specimen dimensions. The fracture toughness of the brittle SHCC matrices (without fiber) is thus determined using linear elastic fracture mechanics (LEFM) considerations, as has been widely used in previous studies and recommendations [13,15,31,32]. The stress intensity factor, K_{Ic}, is given by Eqs. (1)–(4):

$$K_{Ic} = \frac{1.5 \bullet F_{max} \bullet S\sqrt{\pi a}}{BW^2} f(a) \tag{1}$$

where F_{Max} is the highest applied load [N], B is the specimen width [mm], W is the specimen depth [mm], S is the loading span [mm], a is the notch depth and $\alpha = a/W = 0.3(0.05 \leq \alpha \leq 0.8)$ is the relative notch depth ratio. The geometry dependent function $f(a)$ is determined using two-dimensional plane stress analysis and is given by:

$$f(a) = f_1(a) + f_2(a) \tag{2}$$

Where:

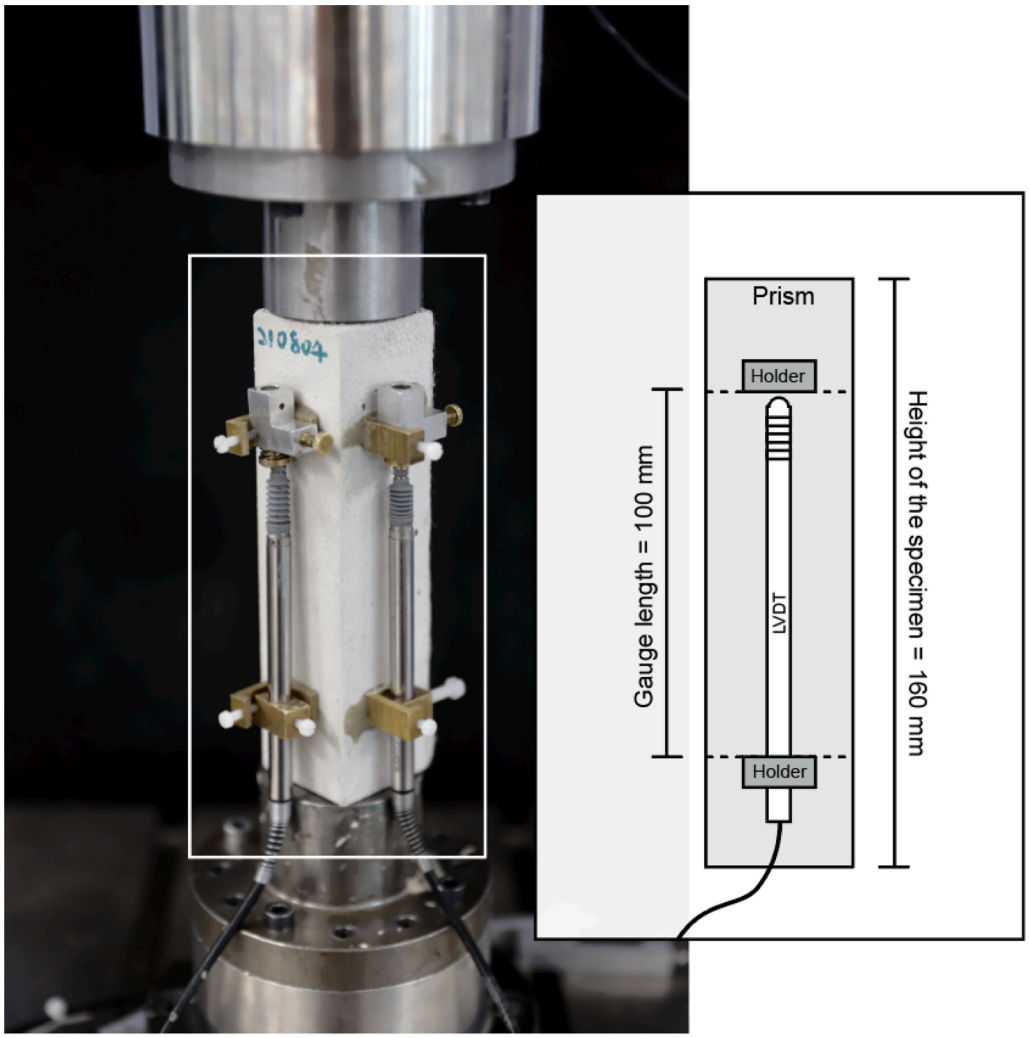

Fig. 3. Experimental set-up for elastic modus test.

$$f_1(a) = \frac{0.68 - 0.744\alpha}{1 - 2.155\alpha + 1.161a^2} \tag{3}$$

$$f_2(a) = 0.36 - 2.088\alpha + 4.611a^2 - 6.499\alpha^3 + 4.233a^4 \quad (for\, 0.05 \le \alpha \le 0.8) \tag{4}$$

Additionally, crack tip toughness J_{tip} (*i.e.*, the critical strain energy release rate) should also be calculated to provide insights from an energy perspective:

$$J_{tip} = \frac{{K_m}^2}{E_m} \tag{5}$$

where E_m is the elastic modulus of the paste [GPa].

The interface properties were determined using single fiber pullout tests following previous studies by Redon et al. [33]. A micromechanics-based model proposed by Lin et al. [34] was adopted to describe the bond properties through the notions of: (1) chemical bond strength G_d quantified by interfacial fracture toughness, (2) constant frictional bond strength τ_0 for small sliding and (3) slip hardening coefficient β that characterizes the increasing effective frictional bond during large sliding (pullout) stage. The tests were performed by using a micro tension-compression testing device from Kammrath & Weiss GmbH as shown in Fig. 4. During the test, both the bottom surface of the thin specimen and the free end of the PVA fibers were glued to two small metal blocks, which were then clamped with the actuator and the load cell (50 N capacity), respectively. The pull-out process was carried out at a displacement rate of 0.005 mm/s, which is identical to the rate of the tensile test. At least 10 specimens were tested for each mixture, the results of which were then analyzed to determine the interface properties (*i.e.*, chemical bond G_d, frictional bond τ_0, and slip-hardening coefficient β) according to Eqs. (6)–(8):

$$G_d = \frac{2(P_a - P_b)^2}{\pi^2 E_f d_f^3} \tag{6}$$

$$\tau_0 = \frac{P_b}{\pi d_f L_e} \tag{7}$$

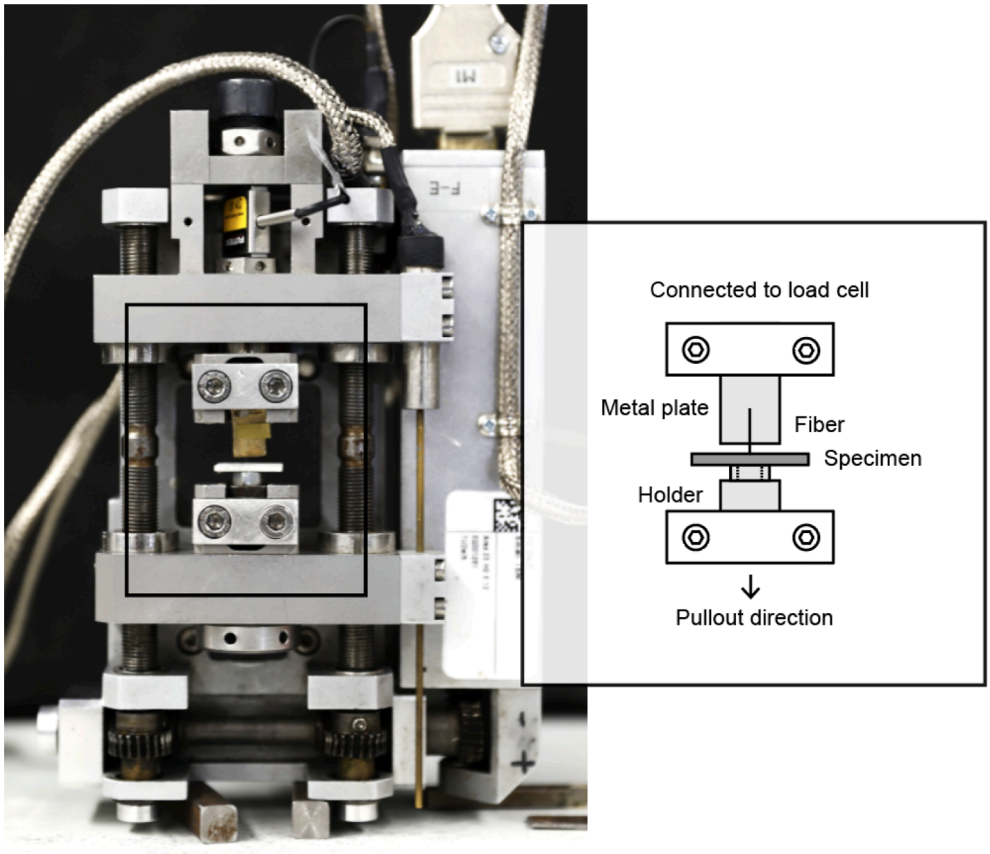

Fig. 4. Experimental set-up for single fiber pullout test.

$$\beta = \frac{d_f}{L_e}\left(1 + \frac{1}{\pi\tau_0 d_f}\cdot\frac{\Delta P}{\Delta u}|_{u\to 0}\right) \tag{8}$$

where E_f, d_f and L_e are the elastic modulus [GPa], diameter [mm], and embedded length of PVA fiber [mm], respectively. $\Delta P/\Delta u$ is the initial slope of the pullout load vs displacement. P_a is the load up to full debonded length and P_b is the load when the fiber begins to slip.

Optical microscope (OLYMPUS BX51) and environmental scanning electron microscope (SEM, QUANTA FEG 450) were used to study the microstructure of interface between PVA fiber and SHCC matrices. The specimens were prepared by cleaving through the fiber so that the fiber/matrix interface was exposed longitudinally.

2.4. Micromechanics-based modelling

Micromechanical modelling based on fracture mechanics provides an opportunity of tailoring micro-parameters and thus modification of the failure mode, the tensile strength, and ultimate tensile strain of composite material [35]. In this study, the micromechanical modelling was performed using a modified fiber bridging constitutive law developed by Yang et al. [36]. The model links the single fiber/matrix interaction to the fiber bridging behavior of a single crack (σ–δ relationship), and the simulated results are used to evaluate the potential for PSH of composite material as described in the following paragraphs. The most important simulated results from the model are the σ-δ relationships of single fiber bridging.

Tensile strain hardening of cement-based material is a result of sequential development of steady-state cracks. The condition for steady-state cracking was quantitatively analyzed by Marshal and Cox based on the J-integral method, which can be expressed as Eq. (9).

$$\frac{{K_m}^2}{E_m} = J_{tip} \le \sigma_0\delta_0 - \int_0^{\delta_0}\sigma(\delta)d\delta \equiv J_b^{'} \tag{9}$$

It indicates that the complementary energy of fiber-bridging $J_b^{'}$ must exceed the crack tip toughness J_{tip}. By assuming the break down zone size of the matrix is small, J_{tip} can be interpreted as the amount of energy consumed in the fracture process G_f and therefore can be calculated by ${K_m}^2/E_m$ at small fiber content as shown in Eq. (9), where K_m is the matrix fracture toughness and E_m is the matrix Young's modulus. The $\sigma(\delta)$ curve, which can be viewed as the constitutive law of fiber-bridging behavior, can be expressed as a function of a set of micromechanics parameters including interface frictional bond strength τ_0 and snubbing coefficient f accounting for the interaction between fiber and matrix when pulled at an inclined angle. Besides interfacial properties, the $\sigma(\delta)$ curve is also governed by the matrix Young's modulus E_m, fiber content V_f, fiber diameter d_f, fiber length L_f, and fiber Young's modulus E_f. In addition, the fiber-bridging strength σ_0 along the crack plane must be higher than the matrix cracking strength σ_c to allow the initiation of crack propagation from a matrix flaw. This consideration leads to the second criterion for strain hardening as Eq. (10).

$$\sigma_c \le \sigma_0 \tag{10}$$

Equations (11) and (12) are referred to as the energy criterion and the strength criterion of pseudo strain hardening, respectively. Satisfaction of both is necessary to achieve tensile strain hardening behavior. The pseudo strain hardening (PSH) performance indices are often used to quantitatively evaluate the likelihood and robustness of strain hardening behavior [14].

$$PSH_{energy} = \frac{J_b^{'}}{J_{tip}} \tag{11}$$

$$PSH_{strength} = \frac{\sigma_0}{\sigma_c} \tag{12}$$

Theoretically, if both PSH indices are larger than 1, strain hardening behavior would occur. However, large margins are preferred to ensure saturated multiple cracking and high tensile strain capacity because of the material heterogeneity. In this study, the measured interface bond properties from the single fiber pullout tests and measured matrix properties were used to calculate fiber-bridging constitutive law and to determine the PSH indices of the SHCC with and without HA.

Table 3
Results of uniaxial compression and tension tests.

Mixture ID	28-day compressive strength (MPa)	First cracking strength (MPa)	Ultimate tensile strength (MPa)	Ultimate tensile strain (MPa)	Residual crack width (μm)
SHCC-0HA	62.8 ± 4.5	3.5 ± 0.2	4.8 ± 0.2	4.8%±0.5%	44.4 ± 33.6
SHCC-1.25HA	59.3 ± 2.1	3.4 ± 0.2	4.4 ± 0.3	4.7%±0.4%	33.6 ± 25.2
SHCC-2.5HA	52.3 ± 1.5	3.4 ± 0.3	4.3 ± 0.3	4.4%±0.3%	25.9 ± 22.5
SHCC-5HA	41.1 ± 2.4	3.0 ± 0.1	4.6 ± 0.2	5.1%±0.7%	13.2 ± 5.3

3. Results and discussion

3.1. Composite performance of SHCC with and without healing agent

Table 3 summarizes the mechanical properties of SHCCs with different amount of HA and the corresponding control mix where no HA was added. Fig. 5 shows the development of compressive strength of the mixtures. As can be seen, the inclusion of HA resulted in strength reductions at all ages. The degree to which the strength was reduced depends on the dosage of HA and the maturity of the specimens. In general, higher dosage of HA leaded to more strength reduction; and the reduction was more pronounce at early ages. One of the possible reasons for this detrimental effect can be due to the hydrolytic degradation of PLA. It has been reported that in aqueous solutions PLA can experience hydrolytic degradation via random cleavage of the ester bond [37]. Depolymerization via hydrolysis leads to the formation of lactic acid, which is likely to consume alkalinity when the HA is mixed with the fresh paste. Since the hydration of slag also demands hydroxyl and alkali ions, a competition may have occurred. It is therefore expected that the use of a higher HA content will lead to greater competition, resulting in a more significant strength reduction.

Fig. 6 shows the tensile stress-strain curves of SHCCs without HA and with the highest dosage of HA (*i.e.*, 5% by weight of binder). As can be seen, both mixes exhibited pronounced tensile strain hardening behavior. Three distinctive phases can be observed in the tensile stress-strain curves. The first phase is the initial elastic stretching phase, during which a linear line with a slope equal to the elastic modulus of the material can be noted. The second phase starts from the formation of the first crack, after which the load continues to increase without damage localization. The sequential formation of multiple parallel cracks (as shown in Fig. 7) results in the transitory load drops and contributes to the inelastic deformation during the strain hardening stage. The third phase begins with the occurrence of the final fracture when the fiber-bridging capacity is exhausted, which defines the ultimate strength of the composite. The corresponding strain value is the tensile strain capacity of the composite.

As shown in Fig. 8a, different from the effect of adding HA to the compressive strength, the tensile strengths (*i.e.*, the first cracking strength and the ultimate tensile strength) were only slightly altered by the addition of HA. When 5% of HA was added, the first cracking strength and the ultimate tensile strength decreased by only 14% and 4%, respectively. The first cracking strength is dependent on the flaw size distribution and the matrix fracture toughness. It is therefore possible that the HA may have served as artificial flaws, for that both the strength and stiffness of PLA are much lower than that of the cement matrix. Once the cracks form, the load shed by the matrix is taken over by the bridging fibers on each crack plane. Therefore, the increase in ultimate tensile strength should be a direct consequence of having enhanced fiber bridging capacity, indicating the formation of stronger fiber/matrix bond. Similarly, the tensile strain capacity of SHCC was also found to be insensitive to the addition of HA. With increasing amount of HA, the tensile strain capacity fluctuated between 4.4% and 5.1%. In fact, the tensile strain was the largest (*i.e.*, 5.1%) when the dosage of HA was the highest. It is therefore concluded that the addition of HA up to 5% by weight to binder did not pose any detrimental effect to the desired tensile properties of SHCC. In the design of self-healing SHCC, the optimal dosage of HA can then be decided purely based on the healing performance.

Furthermore, residual crack width of SHCC was found to decrease with increasing amount of HA as shown by Fig. 9. As summarized in Table 3, compared with the control SHCC without HA, the average crack width of SHCC with 5% HA decreased by 70% from 44.4 μm to 13.2 μm, indicating that the interface frictional bond strength may have been enhanced, which restrains the slippage of the fiber during pullout [16,38]. The observed reduction in crack width is in line with the tensile stress-strain curves as shown in Fig. 6, which shows smaller drops in the stress strain curves when a crack occurs in the case of HA. This unforeseen effect of adding HA is expected to be extremely beneficial to the healing performance of the composite, for which the tight crack width can largely promote the speed and the extend of cracking healing.

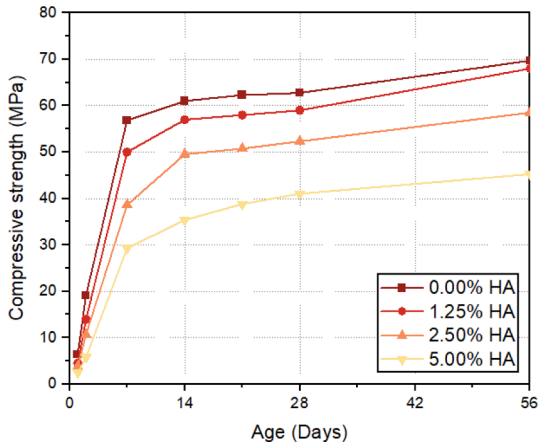

Fig. 5. Compressive strength of SHCCs with different amount of healing agent.

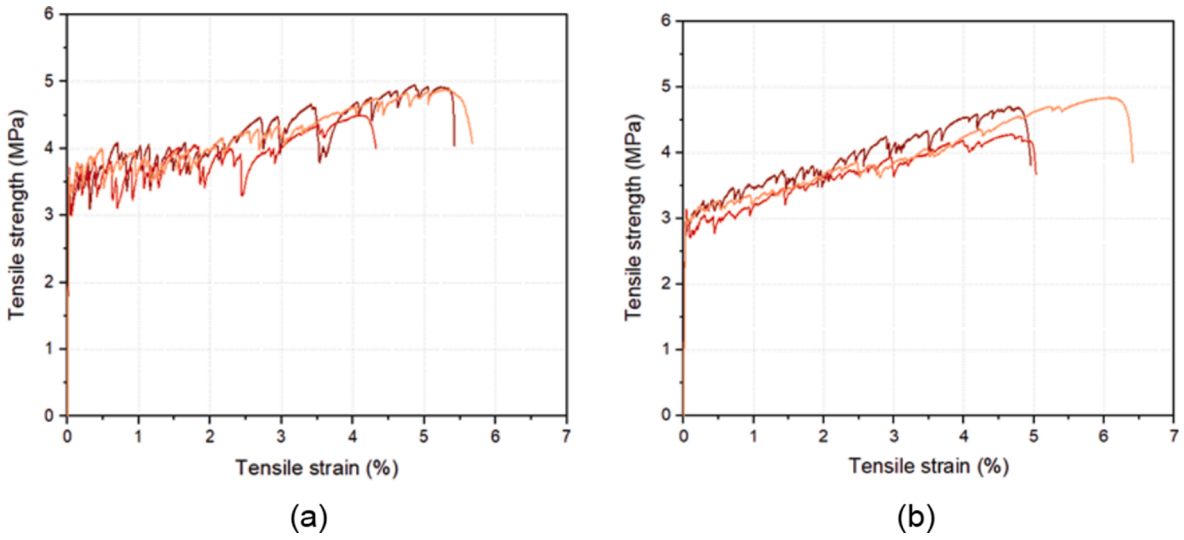

Fig. 6. Representative tensile stress-strain curves of SHCCs (a) without HA and (b) with 5% HA.

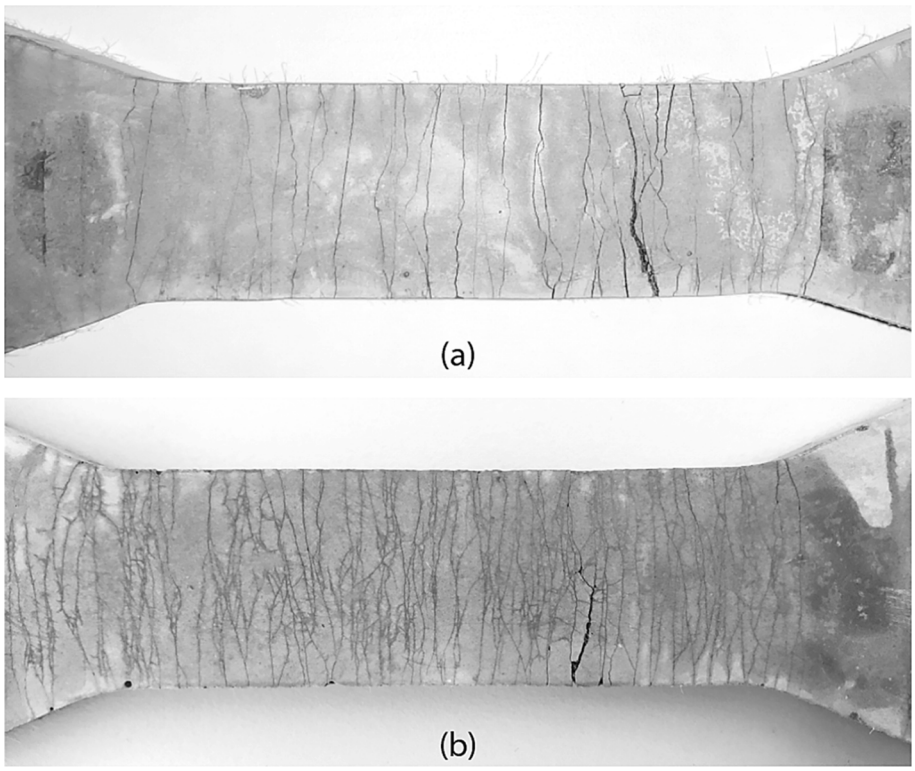

Fig. 7. Typical crack pattern of SHCCs (a) without HA and (b) with HA (gauge length: 8 cm).

3.2. SHCC matrix properties with and without healing agent

Based on the design theory of SHCC as explained in Section 2.4, the tensile strain capacity is determined by both matrix and fiber/matrix interface properties when the same type of fiber is used. Therefore, the effects of HA on the matrix properties were also investigated and the results are summarized in Table 4. Figs. 10 and 11 show the change of fracture toughness and elastic modulus of the SHCC matrices with increasing amount of HA. As can be seen, when the amount of HA was no more than 2.5%, both matrix properties were not noticeably modified. When the dosage was increased to 5%, however, the elastic modulus of the matrix decreased by 31.5% and the fracture toughness increased by 60.1%, as compared to the control SHCC without HA. The reduction in elastic

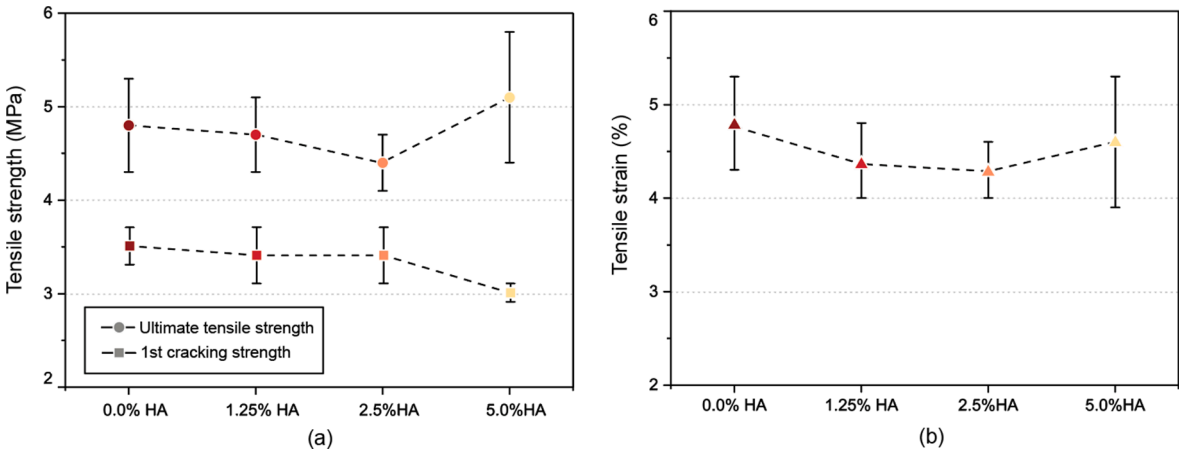

Fig. 8. Results of uniaxial tensile tests of SHCCs.

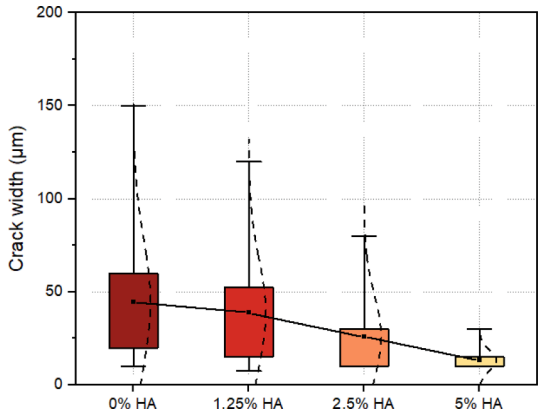

Fig. 9. Residual crack width of SHCCs with different amount of HA.

modulus is as expected, for that the elastic modulus of PLA itself is significantly lower than that of cement hydration products and aggregates. Also, since the addition of HA will inevitably introduce an interfacial transition zone (ITZ) between the particle and the matrix, the formation of porous ITZ will also reduce the stiffness of the resulting composite. The increase in fracture toughness can be attributed to the relatively large particle size of the HA as compared to that of cement and limestone powder. The inclusion of particles of millimeter size can significantly increase the tortuosity of a crack path, leading to higher fracture resistance. In addition, since surface of some HA will experience alkali hydrolysis, the chemical compositions of the hydration product may also be modified. In fact, it has been reported that a strong positive correlation was identified between the Ca/Si ratio of calcium aluminate silicate hydrate (CASH) and its fracture properties [39]. Therefore, since the addition of HA also brings in extra calcium ions, the increase in fracture toughness can also be partially attributed to the increase of Ca/Si ratio of hydration products. It should be noted that the current calculation of the matrix fracture toughness was made under assumption that the LEFM holds true for the brittle SHCC matrices. Therefore, although these fracture data are generally consistent with expected trends, they are probably not the true fracture toughness and should be regarded as indicative values only.

3.3. *Fiber/matrix interface properties*

Besides matrix properties, the fiber/matrix interface properties are also critical to the tensile strain-hardening performance of SHCC. Fig. 12 presents the typical single fiber pullout curve of PVA fiber from SHCC matrix, from which the interface bond properties including chemical bond (G_d), frictional bond strength (τ_0), and slip-hardening coefficient (β) can be derived. The results are summarized in Table 4. As can be seen, both chemical bond and frictional bond increased with increasing HA content. The addition of 5% HA resulted in a 45% enhancement of the chemical bond energy and an 86% enhancement of frictional bond strength. The increase of the bond properties is line with the reduction trend of the residual crack width as measured. The slip-hardening coefficient was not significantly influenced.

To investigate the mechanism for the bond improvement, specimens containing a single fiber were prepared and cleaved at the

Table 4
Matrix and interface bond properties of the SHCCs.

Mixture ID	Matrix properties				Fiber/matrix interface properties		
	Peak force (kN)	Fracture toughness (kPa·m$^{1/2}$)	Elastic modulus (GPa)	Crack tip toughness (J/m^2)	Chemical bond energy Gd (J/m^2)	Frictional bond τ_0 (MPa)	Slip-hardening coefficient β
SHCC-0HA	0.260 ± 0.036	0.143 ± 0.018	16.5 ± 1.4	1.21	4.98 ± 2.42	1.98 ± 0.54	0.302 ± 0.07
SHCC-1.25HA	0.263 ± 0.029	0.144 ± 0.015	17.4 ± 0.3	1.18	5.65 ± 2.38	2.04 ± 1.01	0.235 ± 0.13
SHCC-2.5HA	0.253 ± 0.042	0.139 ± 0.025	17.2 ± 1.1	1.13	6.60 ± 2.31	3.59 ± 1.31	0.241 ± 0.09
SHCC-5HA	0.416 ± 0.013	0.229 ± 0.007	11.3 ± 0.1	4.6	7.20 ± 3.12	3.69 ± 1.49	0.281 ± 0.11

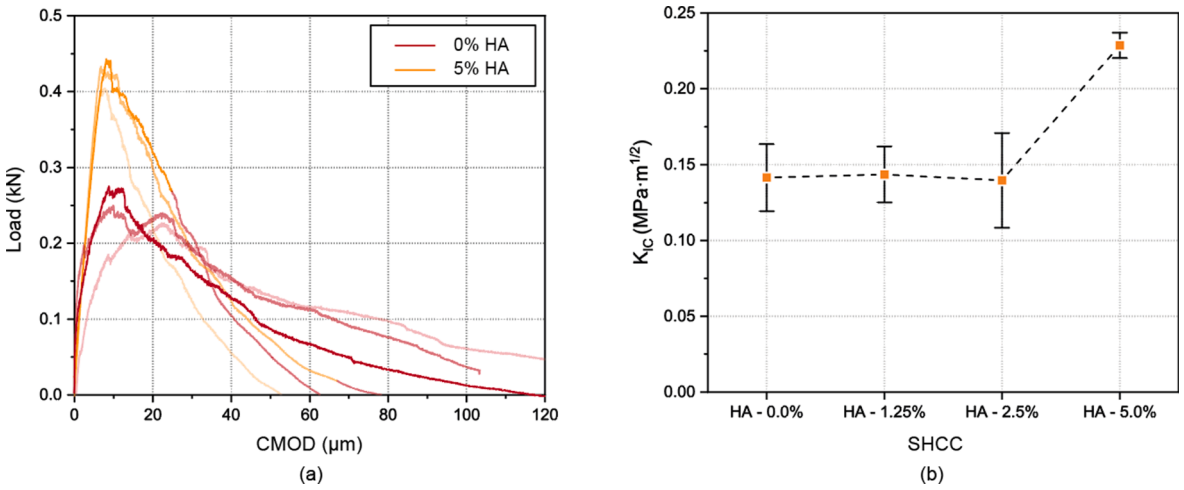

Fig. 10. Results of 3-Point-Bending test: (a) representative Load vs CMOD curves and (b) fracture toughness of SHCC matrices with different amount of HA.

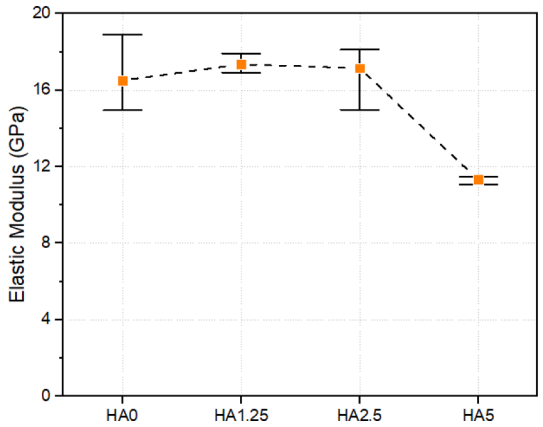

Fig. 11. Young's modulus of SHCC matrix properties.

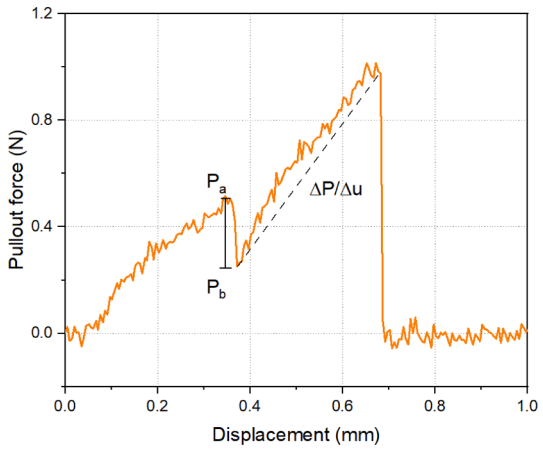

Fig. 12. Representative results of single fiber pullout test.

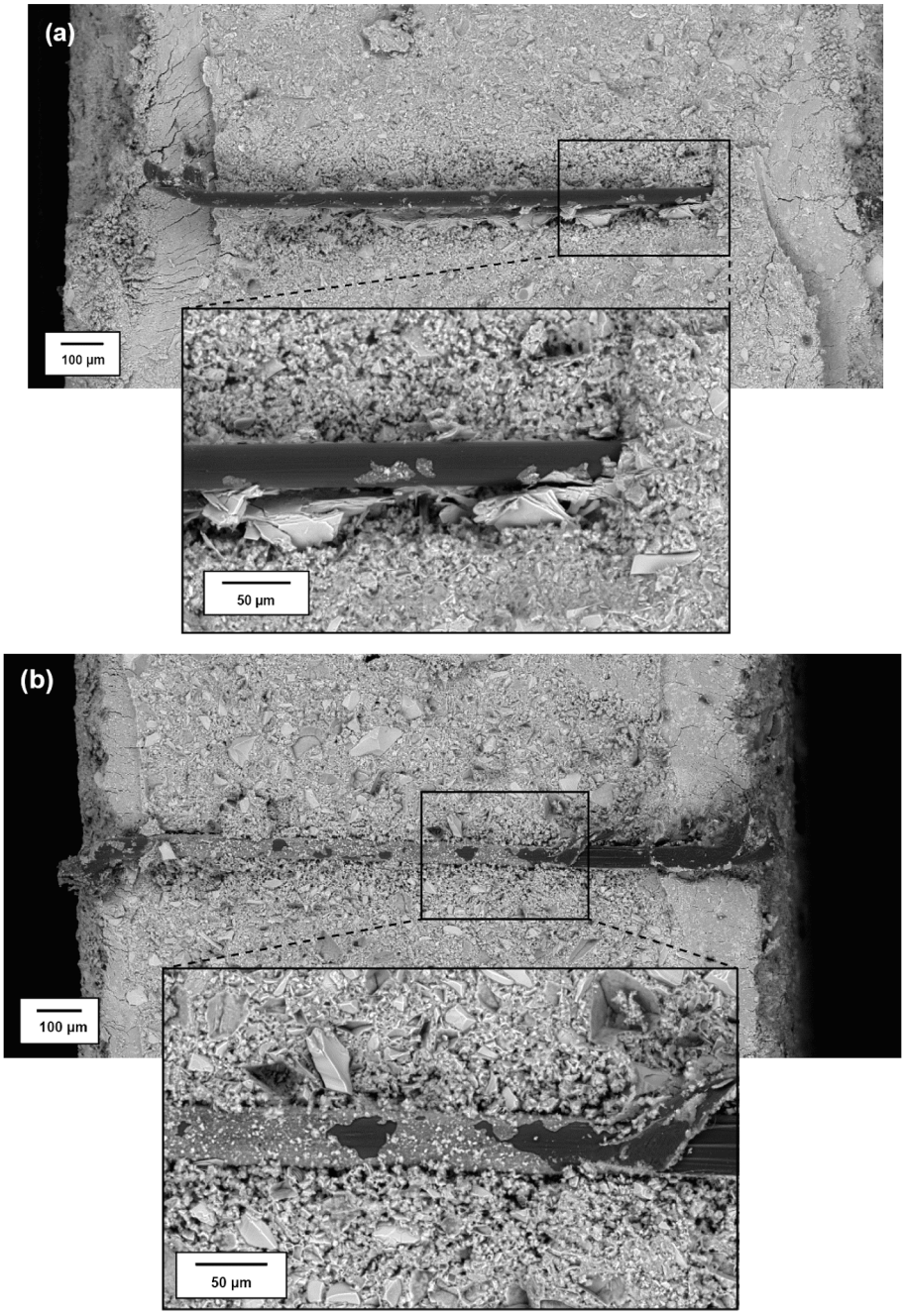

Fig. 13. SEM micrographs of ITZs between fiber and SHCC matrix (a) without HA and (b) with 5% HA.

fiber plane. A longitudinal section of the fiber/matrix ITZ can then be exposed the for SEM analysis. Fig. 13a and b show the resulting, representative micrographs of SHCC matrices having 0% and 5% HA with a fiber partially embedded in the middle (horizontally). As can be seen, the microstructure of the ITZ for specimen with HA is dense, while for the specimen without HA, a very porous zone filled with hexagonal calcium hydroxide (CH) crystals near the fiber can be identified. An ITZ with higher stiffness and compactness will result in more of the contact area and damage tolerance during fiber pullout and therefore led to increased frictional bond strength. The formation of less CH may be attributed to the hydrolytically degradable nature of the PLA. The hydrolysis of a polyester such as PLA produces shorter chains with acid and alcohol terminal groups. The chain cleavage results in a shorter polymer chain and an increasing carboxylic acid-end group concentration, which may have consumed the CH and delayed its precipitation. Further study should be carried out to investigate this densification process. Furthermore, the surface condition of fiber in the two specimens were also very different. In the specimen with HA, a layer of hydration product on the surface of PVA fiber can be easily identified, while the

fiber in specimen without HA had a very smooth and clear surface. This suggests that the matrix with HA have possessed higher chemical affinity with the PVA fiber, which may have contributed to the enhanced chemical bond energy.

3.4. Micromechanics-based modelling of strain hardening potential

The fiber bridging behavior of SHCC with different amount of HA can be calculated based on the measured micromechanical parameters (Table 4) and the fiber parameters provided by the manufacturer (Table 2). Model results of the calculation of complementary energy $J_b^{'}$, peak fiber-bridging strength σ^0 and two *PSH* indices based on the micromechanical model are reported in Table 5. As can be seen, all SHCC mixtures possessed *PSH* indices larger than one regardless the amount of HA. This suggests that all materials satisfied the criteria of achieving the strain hardening performance. However, with increasing amount of HA, the two *PSH* indices exhibited opposite trends. While the *PSH* strength index increased with increasing amount of HA, the PSH energy index decreased significantly from 15 to 3.8. In theory, high indices (*i.e.*, large margins between $J^{'b}$ and J^{tip} and between σ^0 and σ_c) are often necessary to accommodate expected variability and inhomogeneity of the material. Therefore, the decreasing trend of PSH energy index suggests that the addition of HA can deplete the potential of having pronounced strain-hardening behavior. The reason why the SHCCs developed in the current study did not experience any strength and ductility losses with increasing amount of HA is because the potential was not exhausted. But it is possible that tensile properties of SHCC can be attenuated when too much of HA is added. It should be the noted that the required amount of HA may depend on specific application and the required level of healing performance. Even if a strong self-healing performance is demanded, the required dosage of HA may not exceed the highest dosage as adopted in the current study. When the amount of HA is 5% by weight of binder, the equivalent dosage of HA is 51 kg/m^3, whereas the typical dosage used in commercial self-healing concrete is only between 5 to 7.5 kg/m^3. Therefore, it can be concluded that a robust self-healing function can indeed be realized in SHCC without sacrificing its superior tensile properties.

It should be noted that the discovered ITZ strengthening effect of the HA may not always be beneficial to the tensile properties of the SHCC. Especially for SHCC adopting hydrophilic fibers, a perfect bond does not necessarily lead to improved tensile performance because this increases the risk of having extensive fiber rupture. Since fiber pullout rather than rupture confers a larger ductility to the fiber reinforced composites, the bond properties should always be carefully tailored based on the fiber properties and matrix properties to minimize fiber rupture during pullout. For the current study, the reason why the improved bond properties contributed to improved tensile performance of the SHCC is because, for the SHCC mixtures without HA, the strength of the fiber was not fully utilized. Nevertheless, for the group of SHCC utilizing hydrophobic fibers, adding HA into the mixture can always be an effective solution to enable the self-healing functionalities while at the same time improve the tensile and cracking performance of the resulting composites.

4. Conclusion

In this study, the effects of adding bacteria-embedded PLA capsules on mechanical properties of SHCC were investigated. Self-healing SHCC mixtures with different dosages of PLA capsules ranging from 1.25% to 5% by weight of binder were developed; and their mechanical properties were tested and compared with control SHCC without HA. Tests considering behaviors of SHCC mixtures at multiple scales (*i.e.,* at composite, matrix, and fiber/matrix bond level) were performed. It should be noted that, in this study, the self-healing performance was not investigated yet. This will be done in the continuation of the project. The main findings of the current study are:

- The inclusion of the PLA-HA up to 5% by weight to binder did not influence the tensile properties (*i.e.*, tensile strength and ductility) of SHCC. All mixtures exhibited pronounced strain-hardening behavior.
- The residual crack width was found to reduce with increasing HA content. Compared with the control SHCC without HA, the average crack width of SHCC with 5% HA decreased by 70% from 44.4 μm to 13.2 μm. Having smaller crack widths in an SHCC with HA should also result in a better healing capacity.
- The matrix properties (*i.e.*, fracture toughness and elastic modulus) of the SHCC were found to be insensitive to the addition of small and moderate amounts of HA but can change dramatically when the dosage was high. The crack tip toughness of the matrix containing 5% of HA is 3.8 times of that without any HA.
- Single fiber pullout results show that the fiber/matrix bond properties were enhanced by the addition of the HA, which can be attributed to the formation of a denser interfacial transition zone (ITZ) with reduced calcium hydroxide crystals. The improved

Table 5
Results of micromechanical model calculation.

Mixture ID	J_b' (J/m^2)	σ_0(MPa)	J_{tip} (J/m^2)	σ_c(MPa)	PSH strength ($J_b^{'}/J_{tip}$)	PSH energy (σ_0/σ_c)
HCC-0HA	18.16	5.89	1.21	3.5	1.68	15.0
SHCC-1.25HA	16.58	5.78	1.18	3.4	1.70	14.1
SHCC-2.5HA	14.15	6.58	1.13	3.4	1.93	12.5
SHCC-5HA	17.64	6.48	4.6	3.0	2.16	3.8

bond properties led to higher fiber bridging capacity, smaller crack widths and thus partially sustained the tensile strain capacity as verified by the micromechanical model.

CRediT authorship contribution statement

Shan He: Conceptualization, Data curation, Formal analysis, Investigation, Methodology, Validation, Visualization, Writing – original draft. **Shizhe Zhang:** Writing – review & editing, Software, Data curation, Conceptualization. **Mladena Luković:** Conceptualization, Methodology, Supervision, Writing – review & editing. **Erik Schlangen:** Writing – review & editing, Supervision, Project administration, Funding acquisition, Conceptualization.

Declaration of Competing Interest

The authors declare that they have no known competing financial interests or personal relationships that could have appeared to influence the work reported in this paper.

Acknowledgements

This project has received funding from the European Union's Horizon 2020 research and innovation programme under the Marie Sklodowska-Curie grant agreement No 860006. In addition, the authors would like to thank Green-Basilisk BV for providing the healing agent. Also, the authors would like to thank the Advanced Civil Engineering - Materials Research Lab (ACE-MRL), University of Michigan, Ann Arbor for the help with micromechnical modelling. The authors are particularly grateful for the help from Dr. Motohiro Ohno and Dr. Ravi Ranade in programing the micromechanical model of crack-bridging relations.

References

[1] van den Heede P, Mignon A, Habert G, de Belie N. Cradle-to-gate life cycle assessment of self-healing engineered cementitious composite with in-house developed (semi-)synthetic superabsorbent polymers. Cem Concr Compos 2018;94:166–80. https://doi.org/10.1016/J.CEMCONCOMP.2018.08.017.
[2] Van Belleghem B, Van den Heede P, Van Tittelboom K, De Belie N. Quantification of the service life extension and environmental benefit of Chloride Exposed Self-Healing Concrete. Materials 2017;10. https://doi.org/10.3390/MA10010005.
[3] Huang H, Ye G, Damidot D. Effect of blast furnace slag on self-healing of microcracks in cementitious materials. Cem Concr Res 2014;60:68–82. https://doi.org/10.1016/J.CEMCONRES.2014.03.010.
[4] Yang Y, Lepech MD, Yang E-H, Li VC. Autogenous healing of engineered cementitious composites under wet–dry cycles. Cem Concr Res 2009;39:382–90. https://doi.org/10.1016/J.CEMCONRES.2009.01.013.
[5] De Nardi C, Bullo S, Ferrara L, Ronchin L, Vavasori A. Effectiveness of crystalline admixtures and lime/cement coated granules in engineered self-healing capacity of lime mortars. Mater Struct 2017;50:1–12. https://doi.org/10.1617/s11527-017-1053-3.
[6] Ferrara L, Krelani V, Carsana M. A "fracture testing" based approach to assess crack healing of concrete with and without crystalline admixtures. Constr Build Mater 2014;68:535–51. https://doi.org/10.1016/J.CONBUILDMAT.2014.07.008.
[7] Wang JY, Soens H, Verstraete W, de Belie N. Self-healing concrete by use of microencapsulated bacterial spores. Cem Concr Res 2014;56:139–52. https://doi.org/10.1016/J.CEMCONRES.2013.11.009.
[8] Van Mullem T, Anglani G, Dudek M, Vanoutrive H, Bumanis G, Litina C, et al. Addressing the need for standardization of test methods for self-healing concrete: an inter-laboratory study on concrete with macrocapsules. Sci Techn Advan Mater 2020;21:661–82. https://doi.org/10.1080/14686996.2020.1814117.
[9] Shields Y, De Belie N, Jefferson A, Van Tittelboom K. A review of vascular networks for self-healing applications. Smart Mater Struct 2021;30:063001. https://doi.org/10.1088/1361-665X/ABF41D.
[10] Jonkers HM, Thijssen A, Muyzer G, Copuroglu O, Schlangen E. Application of bacteria as self-healing agent for the development of sustainable concrete. Ecol Engng 2010;36:230–5. https://doi.org/10.1016/J.ECOLENG.2008.12.036.
[11] Van Tittelboom K, De Belie N. Self-healing in cementitious materials—A review. Materials 2013;6:2182–217. https://doi.org/10.3390/ma6062182.
[12] de Belie N, Gruyaert E, Al-Tabbaa A, Antonaci P, Baera C, Bajare D, et al. A review of self-healing concrete for damage management of structures. Adv Mater Interfaces 2018;5. https://doi.org/10.1002/admi.201800074.
[13] Li VC. Engineered Cementitious Composites (ECC). Engineered Cementitious Composites (ECC) 2019. https://doi.org/10.1007/978-3-662-58438-5.
[14] Li VC, Leung CKY. Steady state and multiple cracking of short random fiber composites. J Engng Mech 1992;118:2246–64. https://doi.org/10.1061/(ASCE)0733-9399(1992)118:11(2246).
[15] Li VC, Mishra DK, Wu H-C. Matrix design for pseudo-strain-hardening fibre reinforced cementitious composites. Mater Struct 1995;28:586–95. https://doi.org/10.1007/BF02473191.
[16] Li VC, Wu C, Wang S, Ogawa A, Saito T. Interface tailoring for strain-hardening polyvinyl alcohol-engineered cementitious composite (PVA-ECC). Mater J 2002;99:463–72. https://doi.org/10.14359/12325.
[17] Yildirim G, Keskin ÖK, Keskin SBI, Şahmaran M, Lachemi M. A review of intrinsic self-healing capability of engineered cementitious composites: Recovery of transport and mechanical properties. Constr Build Mater 2015;101:10–21. https://doi.org/10.1016/J.CONBUILDMAT.2015.10.018.

[18] Fan S, Li Mo. X-ray computed microtomography of three dimensional microcracks and self-healing in engineered cementitious composites. Smart Mater Struct 2015;24. https://doi.org/10.1088/0964-1726/24/1/015021.
[19] Qiu J, Tan HS, Yang EH. Coupled effects of crack width, slag content, and conditioning alkalinity on autogenous healing of engineered cementitious composites. Cem Concr Compos 2016;73:203–12. https://doi.org/10.1016/j.cemconcomp.2016.07.013.
[20] Mors RM, Jonkers HM. Feasibility of lactate derivative based agent as additive for concrete for regain of crack water tightness by bacterial metabolism. Ind Crops Prod 2017;106:97–104. https://doi.org/10.1016/j.indcrop.2016.10.037.
[21] Tziviloglou E, Wiktor V, Jonkers HM, Schlangen E. Selection of nutrient used in biogenic healing agent for cementitious materials. Front Mater 2017;4. https://doi.org/10.3389/fmats.2017.00015.
[22] Mors R, Jonkers H. Effect on concrete surface water absorption upon addition of lactate derived agent. Coatings 2017;7. https://doi.org/10.3390/coatings7040051.
[23] Mercuri L, Romero Rodriguez C, Xu Y, Chaves Figueiredo S, Mors R, Rossi E, et al. On the role of soft inclusions on the fracture behaviour of cement paste. In: Pijaudier-Cabot G, Grassl P, la Borderie C, editors. 10th International Conference on Fracture Mechanics of Concrete and Concrete Structures (FraMCoS-X), Bayonne: 2019. https://doi.org/10.21012/FC10.235271.
[24] Zhou J, Qian S, Sierra Beltran MG, Ye G, van Breugel K, Li VC. Development of engineered cementitious composites with limestone powder and blast furnace slag. Mater Struct/Materiaux et Constructions 2010;43:803–14. https://doi.org/10.1617/s11527-009-9549-0.
[25] European committee for standardization. NEN-EN 197-1. Cement - Part 1: Composition, specifications and conformity criteria for common cements. 2011.
[26] Carl Redon B, Li VC, Wu C, Hoshiro H, Saito T, Ogawa A. Measuring and modifying interface properties of PVA fibers in ECC matrix n.d.
[27] European committee for standardization. NEN-EN 196-1. Methods of testing cement - Part 1: Determination of strength. 2016.
[28] Rokugo Tetsushi Kanda AE Hiroshi Yokota AE Noboru Sakata KA. Applications and recommendations of high performance fiber reinforced cement composites with multiple fine cracking (HPFRCC) in Japan n.d. https://doi.org/10.1617/s11527-009-9541-8.
[29] European committee for standardization. NEN-EN 12390-13. Testing hardened concrete - Part 13: Determination of secant modulus of elasticity in compression. 2021.
[30] COST Action TU 1404. Main phase of the Extended Round Robin Testing programme for TU1404 - Testing protocols. 2016.
[31] Sonat C, He S, Li J, Unluer C, Yang E-H. Strain hardening magnesium-silicate-hydrate composites (SHMSHC) reinforced with short and randomly oriented polyvinyl alcohol microfibers. Cem Concr Res 2021;142. https://doi.org/10.1016/j.cemconres.2021.106354.
[32] Zhang S, Li VC, Ye G. Micromechanics-guided development of a slag/fly ash-based strain-hardening geopolymer composite. Cem Concr Compos 2020;109. https://doi.org/10.1016/j.cemconcomp.2020.103510.
[33] Redon C, Li VC, Wu C, Hoshiro H, Saito T, Ogawa A. Measuring and modifying interface properties of PVA fibers in ECC matrix. J Mater Civ Engng 2001;13:399–406. https://doi.org/10.1061/(ASCE)0899-1561(2001)13:6(399).
[34] Lin Z, Kanda T, Li V. On interface property characterization and performance of fiber reinforced cementitious composites. Concr Sci Engng 1999;1:173–84.
[35] Li VC. Tailoring ECC for special attributes: A review. Int J Concr Struct Mater 2012;6:135–44. https://doi.org/10.1007/S40069-012-0018-8.
[36] Yang E-H, Wang S, Yang Y, Li VC. concrete VL-J of advanced, 2008 undefined. Fiber-bridging constitutive law of engineered cementitious composites. J Adv Concr Technol 2008;6:181–93.
[37] Elsawy MA, Kim KH, Park JW, Deep A. Hydrolytic degradation of polylactic acid (PLA) and its composites. Renew Sustain Energy Rev 2017;79:1346–52. https://doi.org/10.1016/J.RSER.2017.05.143.
[38] He S, Qiu J, Li J, Yang E-H. Strain hardening ultra-high performance concrete (SHUHPC) incorporating CNF-coated polyethylene fibers. Cem Concr Res 2017;98:50–60. https://doi.org/10.1016/j.cemconres.2017.04.003.
[39] Zhang S, Li Z, Ghiassi B, Yin S, Ye G. Fracture properties and microstructure formation of hardened alkali-activated slag/fly ash pastes. Cem Concr Res 2021;144. https://doi.org/10.1016/j.cemconres.2021.106447.